Simulation Analysis of Transport of Boron Dust Particles Injected by Impurity Powder Dropper in the Large Helical Device

J. Adv. Simulat. Sci. Eng.
Vol. 11, No. 1, 12–20.

Simulation Analysis of Transport of Boron Dust Particles Injected by Impurity Powder Dropper in the Large Helical Device

Mamoru Shoji[1,2*], Gakushi Kawamura[1,2], Roman Smirnov[3], Yasunori Tanaka[4]

[1]National Institute for Fusion Science, National Institutes of Natural Science
[2]Fusion Science Program, Graduate University for Advanced Studies, SOKENDAI
[3]Department of Mechanical and Aerospace Engineering, University of California at San Diego
[4]Institute of Science and Engineering, Kanazawa University

*shohji.mamoru@nifs.ac.jp

Received: January 1, 2024; Accepted: January 23, 2024; Published: February 6, 2024

Abstract. Boron dust particles were injected by an impurity powder dropper to improve plasma confinement and perform wall conditioning in the Large Helical Device. A fast-framing camera for monitoring dust particle trajectories in the peripheral plasma detected a change in the ablation positions of the dust particles depending on the plasma density and heating power. An analysis using a three-dimensional edge plasma simulation code (EMC3-EIRENE) and a dust transport simulation code (DUSTT) was applied to understand these observations. The simulations proved that the dust particle trajectories are more deflected toward the outboard side of the torus by the effect of the plasma flow in an upper divertor leg for higher plasma densities and higher plasma heating powers. The simulation successfully reproduced observations of the change in the ablation positions in the peripheral plasma.

Keywords: Dust transport simulation, Impurity powder dropper, Peripheral plasma, LHD

1. Introduction

Impurity powder injection is going to attract attention as one of the promising methods for real-time wall conditioning, impurity seeding, and dust particle transport studies in magnetic plasma confinement devices [1]. An impurity powder dropper (IPD) [2] was installed at an upper port on the vacuum vessel in the Large Helical Device (LHD) [3]. Ion and electron energy confinement in the plasma was improved by boron dust particle injection using the IPD in previous experimental campaigns [4,5]. It has been suggested that control of the trajectory and ablation positions of the dropped dust particles is a critical issue for demonstrating the potential of the IPD to realize high-performance plasma discharges [6]. This is because the plasma flow in an upper divertor leg deflects the trajectories of the dropped dust particles, by which they cannot

reach the main plasma [7]. The ablation positions of dust particles have been routinely monitored with a fast-framing camera installed in an upper port close to the IPD. For higher plasma densities and higher plasma heating powers, the camera detected the change of the ablation positions toward the outboard side of the torus. The observations are analyzed using a three-dimensional edge plasma simulation code (EMC3-EIRENE) [8,9] and a dust transport simulation code (DUSTT) [10,11,12].

2. Observation of ablation positions of boron dust particles in peripheral plasma

2.1. Dependence of ablation position on plasma density

Figure 1 shows the experimental setup for observing the trajectory of dropped dust particles and the ablation positions. Figure 1(a) presents a poloidal cross-section of a plasma and the vacuum vessel at the toroidal position where the IPD was installed. The IPD has been installed on one of the upper ports (2.5-U). A visible fast-framing camera (Photron FASTCAM SA-X) has been installed in an upper port close to the IPD. Figures 1(b) and (c) give CAD and real images of the plasma and the in-vessel components viewed from the position of the fast-framing camera.

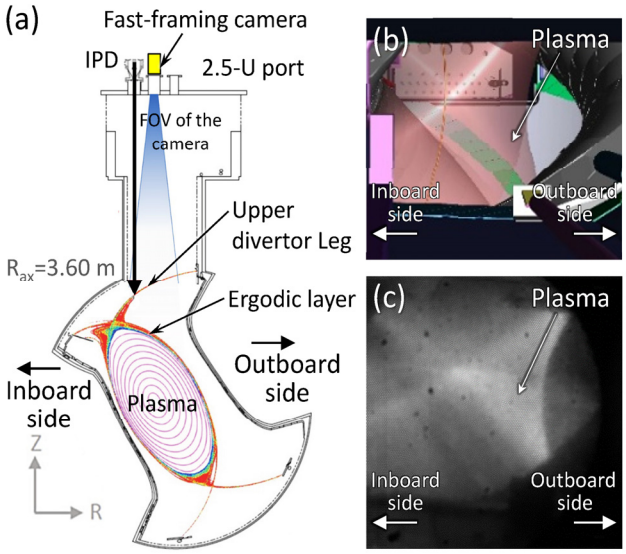

Figure 1: (a) Experimental setup of a fast-framing camera for observing the trajectories and ablation positions of dust particles dropped from the IPD in a typical magnetic configuration (R_{ax}=3.60 m), (b) a CAD image of a plasma and in-vessel components viewed from the position of the camera, (c) a real image observed with the fast-framing camera.

Figure 2 shows snapshots of the image of the ablation cloud of boron dust particles (150 μm in diameter) dropped from the IPD observed with the fast-framing camera. These images were taken at an initial phase of the dust injection for three different plasma densities in hydrogen discharges for a typical magnetic configuration (the radial position of the magnetic axis R_{ax}=3.60 m) at a frame rate of 2,000 fps (the exposure time is 0.5 milliseconds). The total plasma heating power by the NBIs in the plasma discharges was about 10 MW. Here, the heating power is defined as the total port-through power of the NBIs. First, the boron dust particles pass through an upper divertor leg, then they reach the peripheral plasma (so-called ergodic layer) at a toroidal position where the shape of the plasma is almost vertically elongated with a poloidally small counterclockwise rotation as shown in Figure 1(a). The fast-framing camera detected a few moving luminescent spots after the start of the injection, which was produced by interactions between the dust particles and the peripheral plasma. The spots indicate the ablation positions of the dust particles. The images of ablation clouds in Figure 2 were taken at the time when the dust

particles emitted the brightest light. After this, the light rapidly disappears within a few frames, indicating that the positions of the dust particles in this figure almost correspond to the points where the dust particles were completely evaporated/sublimated in the peripheral plasma. It is well known that the ablation clouds expand along magnetic field lines because of the impurity ion transport parallel to the magnetic field. The observed angles of the tail of the ablation cloud are consistent with the pitch angle of the magnetic field line in the ergodic layer, which guarantees the ablation of the boron dust particles in the ergodic layer. The images show that the ablation positions changed toward the outboard side of the torus with an increase in the plasma density. Using scales made by the comparison of the real images with the CAD image (Figure 1(b)) shown in these three figures, the difference of the change in the ablation positions for the three plasma densities can be estimated.

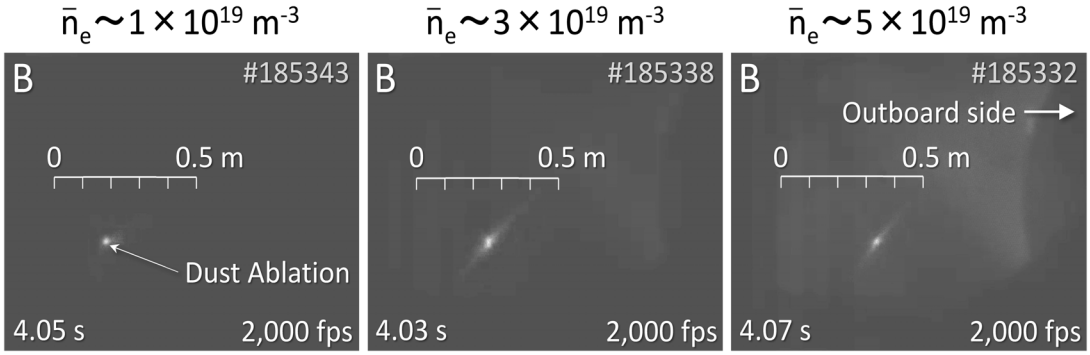

Figure 2: Snapshots of the ablation cloud of boron dust particles dropped from the IPD, which were taken with a fast-framing camera installed in an upper port at an initial phase of the dust injection for three different average plasma densities for R_{ax}=3.60 m.

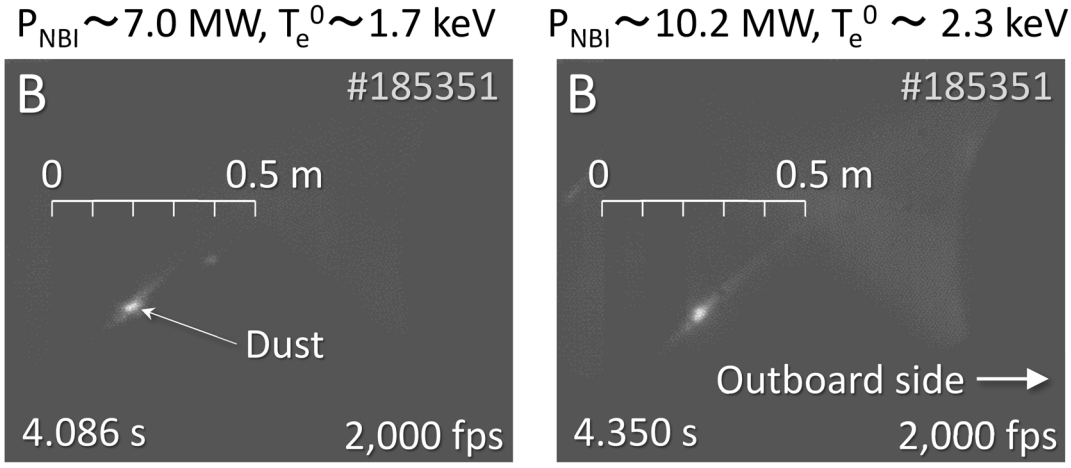

Figure 3: Snapshots of the ablation cloud of dropped boron dust particles, observed with the fast-framing camera for two different plasma heating powers by NBIs (P_{NBI}=7.0 MW and 10.2 MW) in a plasma discharge for R_{ax}=3.60 m. The average plasma density was kept at about 4×10^{19} m^{-3}.

2.2. Dependence of ablation position on plasma heating power

Figure 3 presents snapshots of the ablation cloud of the dropped boron dust particles in two different plasma heating powers for a typical magnetic configuration (R_{ax}=3.60 m) at a frame rate of 2,000 fps. It shows that the ablation positions moved to the outboard side of the torus

with an increase in plasma heating power. The heating power was controlled by adjusting a combination of the injection time of two Neutral Beam Injectors (NBIs) in a plasma discharge in which the average plasma density was kept at about 4×10^{19} m^{-3} by real-time control of hydrogen gas fueling. The total plasma heating power by the NBIs before and after 4.1 seconds was estimated to be about 7.0 MW and 10.2 MW, respectively. In this plasma discharge, the plasma stored energy increased stepwise at 4.1 seconds. The radial profiles of the plasma density just before and after 4.1 seconds were almost the same, meaning that the plasma temperature rose then. A Thomson scattering system detected a temporal stepwise increase in the electron temperature around the plasma center (T_e^0) from about 1.7 keV to 2.3 keV at the time. The scales in these two figures, the difference of the change in the ablation positions for the two plasma heating powers can be recognized.

3. Simulation analysis of transport of dust particles injected by impurity powder dropper

The change in the ablation positions of the dust particles was analyzed using the EMC3-EIRENE code and the DUSTT code. Figure 4 illustrates the perspective view of a three-dimensional model of the vacuum vessel for a one-half helical coil pitch angle (18° in toroidal direction) for this analysis. The figure also shows a poloidal cross-section of a typical peripheral plasma density profile at the toroidal angle where the IPD is installed. The three-dimensional profile of the plasma parameters (plasma density, ion and electron temperatures, and plasma flow velocity, etc.) in the background hydrogen plasma was provided by EMC3-EIRENE for a typical magnetic configuration (R_{ax}=3.60 m) in an open divertor geometry. The input parameters for EMC3-EIRENE are the plasma heating power and the plasma density inside the Last Closed Flux Surface (LCFS) (defined as P^{LCFS} and n_e^{LCFS}, respectively). The perpendicular particle and thermal diffusion coefficients in the peripheral plasma were defined as 0.5 m^2/s and 1.0 m^2/s, respectively. These two values are typical ones for reproducing the observation of the radial profile of the electron temperature and density in the peripheral plasma [13]. A converged solution of the plasma parameter profiles was finally obtained after repeating iterative calculations in the code.

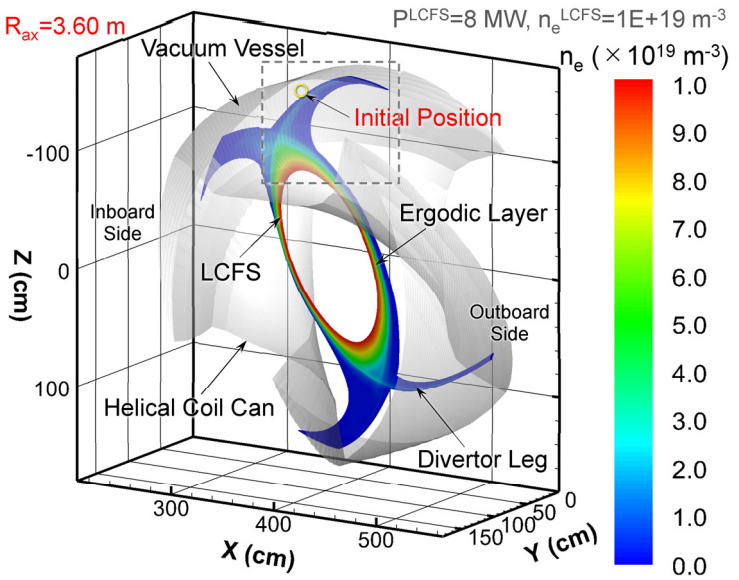

Figure 4: A three-dimensional model for dust particle transport simulation in the peripheral plasma in the LHD using the EMC3-EIRENE code and the DUSTT code. A grey broken square corresponds to the area in Figs. 5-8.

The trajectories of dust particles were calculated by DUSTT under the three-dimensional background plasmas. The code solves

the equation of motion of spherical-shaped dust particles with heat, charge, and mass equations, including the effect of ion/neutral drag force, gravity, and electrostatic force [10,11,12]. The ion drag force is separated into two components. One is the absorption of ions by dust particles which is calculated by the orbital motion limited (OML) theory [14], and another one is by Coulomb's scattering. It is assumed that dust particles are composed of a single atomic element (such as boron) and the shape of dust particles is spherical. In the simulation, the dust particles were dropped from an initial position just above an upper divertor leg with a downward velocity of 5.0 m/s, which corresponds to the speed in the case where the dust particles were dropped from the actual IPD position (outside of the model). The effect of the impurity ion flow produced by the dust particles was not included in the simulation. This assumption is reasonable because the observed ablation clouds were taken in the initial phase of the dust injection (the density of the boron ions in the plasma is quite low). The reflection of the dust particles on the vacuum vessel and the in-vessel components was not considered.

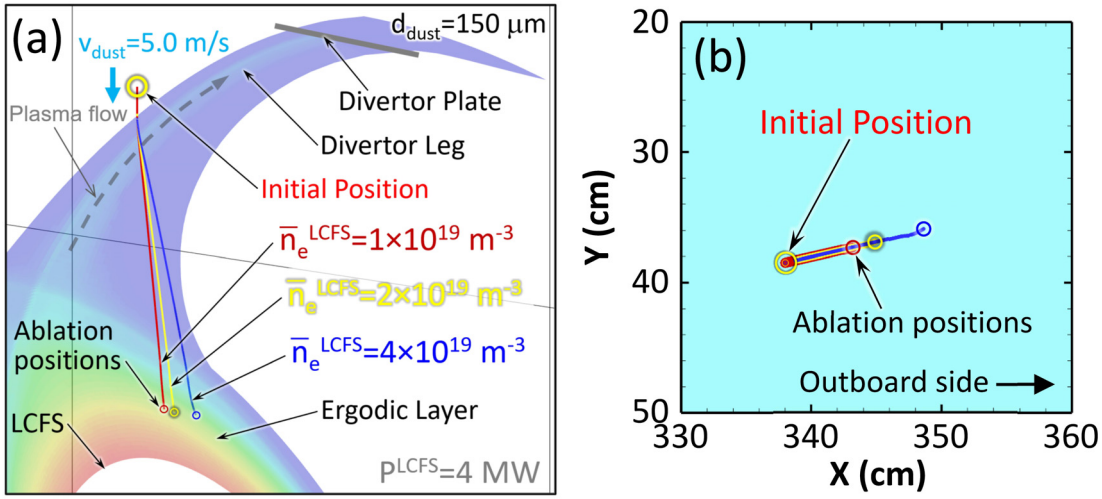

Figure 5: (a) An enlarged view presenting the simulations of the trajectories of boron dust particles (150 μm in diameter) dropped from the IPD for the three different plasma densities (n_e^{LCFS}=1, 2, and 4×10^{19} m^{-3}) for a plasma heating power inside the LCFS (P^{LCFS}=4 MW). (b) A top view of the calculated boron dust trajectories and the ablation positions in the three plasma density cases.

Figure 5(a) presents the simulations of the trajectories of boron dust particles dropped from the initial position for three different plasma densities (n_e^{LCFS}) ranging from 1×10^{19} m^{-3} to 4×10^{19} m^{-3}. The plasma heating power inside the LCFS (P^{LCFS}) was set to 4.0 MW which was a typical heating power in plasma discharge experiments. The diameter of the boron dust particles was set to 150 μm, corresponding to the nominal size used for the experiments. The ablation positions of the dust particles are indicated as open-colored circles in the ergodic layer, in which the ablation positions are defined as the points where the dust particles are completely evaporated/sublimated by the heat load from the plasma. Figure 5(b) is a top view of the boron dust trajectories and the ablation positions in the three plasma density cases in the model. The simulation shows that the plasma flow at the upper divertor leg deflects the trajectories of the boron dust particles [7]. The trajectories are more deflected for the higher plasma densities, which results in the change of the ablation position in the ergodic layer toward the outboard side of the torus. The simulation results of the change in the ablation positions depending on

both parameters presented in Figures 4(b) and 5(b) are approximately consistent with the observed dependences which are shown in Figures 2 and 3.

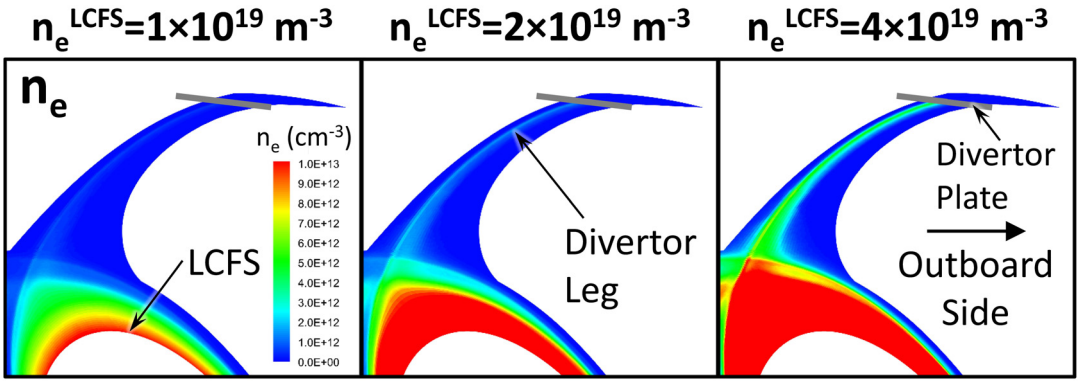

Figure 6: Enlarged views of the poloidal cross-section of the plasma density profile in the upper divertor leg for the three plasma densities (n_e^{LCFS}=1, 2, and 4×10^{19} m^{-3}) with a plasma heating power inside the LCFS (P^{LCFS}) of 4 MW.

Figure 6 gives the enlarged views of the poloidal cross-section of the plasma density profile in the upper divertor leg for the three plasma densities (n_e^{LCFS}=1, 2, and 4×10^{19} m^{-3}). The DUSTT code proved that the ion drag force on dust particles by the plasma flow in the upper divertor leg is the most dominant force affecting the change of the dust particle trajectories. In the simulation code, the ion drag force has a positive dependence on the plasma density [15]. As a result, the simulation using the EMC3-EIRENE code and the DUSTT code has successfully explained the observed dependence of the ablation position on the plasma density.

Figure 7(a) presents the simulations of the trajectories of the dropped boron dust particles for four different plasma heating powers inside the LCFS (P^{LCFS}) ranging from 2 MW to 8 MW. It seems to cover absorbed heating powers in the main plasma in the experimental conditions for the two heating powers by the NBIs (P_{NBI}=7.0 MW and 10.2 MW). The plasma density was

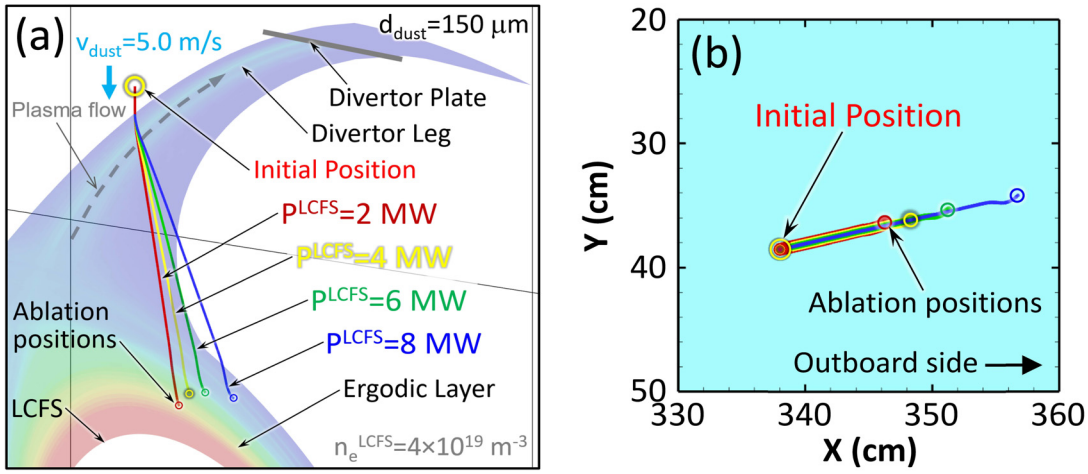

Figure 7: (a) An enlarged view presenting the simulations of the trajectories of boron dust particles (150 μm in diameter) dropped from the IPD for the four different plasma heating powers inside the LCFS (P^{LCFS}=2, 4, 6, and 8 MW) for a plasma density (n_e^{LCFS}) of 4×10^{19} m^{-3}. (b) A top view of the boron dust trajectories and the ablation positions in the four plasma heating power cases.

set to 4×10^{19} m^{-3}, and the diameter of the boron dust particles was set to 150 μm. Figure 7(b) is a top view of the boron dust trajectories and the ablation positions in the four plasma heating power cases in the model. The simulation indicates that the trajectories of the dropped boron dust particles at the upper divertor leg are more deflected for higher plasma heating powers. It causes the change in the ablation position of the dust particles toward the outboard side of the torus in the ergodic layer for the higher plasma heating powers. Consequently, the simulation successfully reproduced the observed change of the ablation positions toward the outboard side with the increase in the plasma heating power.

The reason for the dependence on the plasma heating power is due to the enhanced plasma flow velocity in the upper divertor leg by the increased ion/electron temperature. Numerical calculations of the ion drag force on dust particles, which is the most dominant force affecting the change of the dust particle trajectories at the divertor leg, prove that the force has a positive dependence on the plasma flow velocity in the divertor plasma in LHD [15,16,17]. Figure 8 presents the enlarged views of the poloidal cross-section of the ion temperature (T_i) and the plasma flow velocity (v_p) profile in the upper divertor leg for the four plasma heating powers (P^{LCFS}=2, 4, 6, and 8 MW). The figures show that both parameters increase with the plasma heating power. The plasma flow is determined by the flow velocity on the divertor plates because of the short connection length of the magnetic field lines in the divertor leg [18]. The EMC3-EIRENE code assumes that the flow velocity on the divertor plates is the sound speed, which has a positive correlation with the ion and electron temperature in the plasma. It means that the increased ion/electron temperature enhances the plasma flow velocity in the upper divertor leg, resulting in more deflection of the dropped boron dust particles. As for the drift of the plasma, this effect is negligible for the change in the ablation position because the plasma flow along the magnetic field line is dominant over that by the drift in the divertor leg.

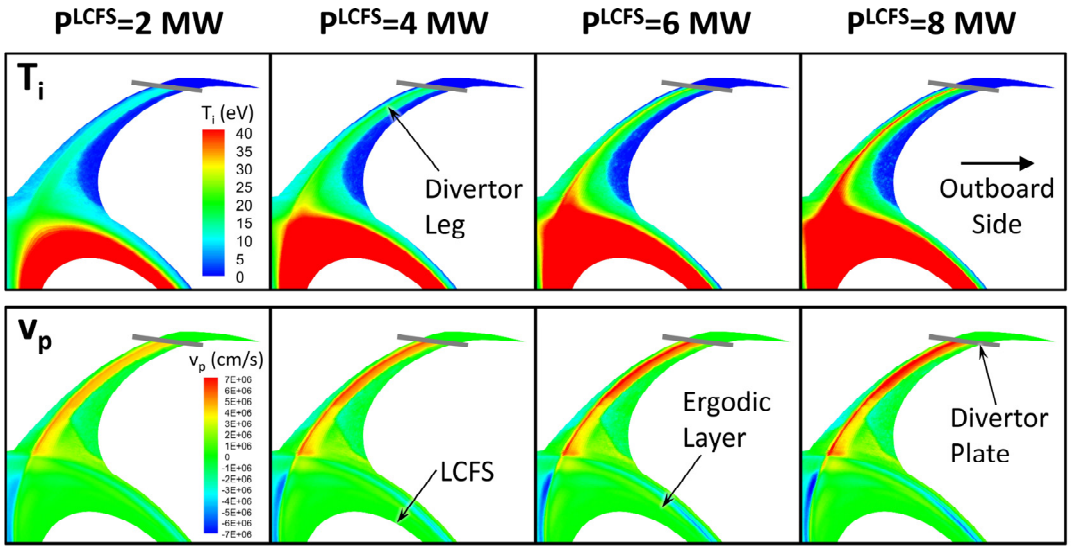

Figure 8: Enlarged views of the poloidal cross-section of the ion temperature (upper) and the plasma flow velocity profile (lower) in the upper divertor leg for the four plasma heating powers inside the LCFS (P^{LCFS}=2, 4, 6, and 8 MW) for a plasma density (n_e^{LCFS}) of 4×10^{19} m^{-3}.

4. Summary

A fast-framing camera detected a change in the ablation position of the boron dust particles dropped from the IPD toward the outboard side of the torus with the plasma density and heating power. These observations were analyzed using a three-dimensional edge plasma simulation code (EMC3-EIRENE) and a dust transport simulation code (DUSTT). The simulation shows that the trajectories of the dropped boron dust particles are more deflected at the upper divertor leg by the effect of the plasma flow for higher plasma densities and higher heating powers. The deflection of the dust particle trajectories results in the change of the ablation positions in the ergodic layer. The simulation successfully reproduced the observed change of the ablation positions for the higher plasma densities and higher heating powers.

Acknowledgments

This work is performed under the auspices of the NIFS Collaboration Research program (NIFS22KIST004). One of the authors (M. Shoji) appreciates members of the Department of Engineering and Technical Services for their dedicated support. He also thanks the computational resources of the plasma simulator in NIFS. This work is helped by a JSPS KAKENHI Grant Number 21K18620. It is also supported by the U.S. Department Of Energy under Contract No. DE-AC02-09CH11466 with Princeton University". One of the authors (R. Smirnov) would like to acknowledge support from the U.S. Department of Energy, Office of Science, Office of Fusion Energy Sciences under Award No. DE-FG02-06ER54852.

References

[1] A. Bortolon, V. Rohde, R. Maingi, et al.: Real-time wall conditioning by controlled injection of boron and boron nitride powder in full tungsten wall ASDEX Upgrade, *Nucl. Mater. Energy*, 19 (2019), 384-389.

[2] A. Nagy, A. Bortolon, D. M. Mauzey, et al.: A multi-species powder dropper for magnetic fusion applications, *Rev. Sci. Instrum.*, 89 (2018), 10K121-1-5.

[3] Y. Takeiri, T. Morisaki, M. Osakabe, et al.: Extension of the operational regime of the LHD towards a deuterium experiment, *Nucl. Fusion*, 57:10 (2017), 102023-1-10.

[4] F. Nespoli, N. Ashikawa, E. Gilson, et al.: First impurity powder injection experiments in LHD, *Nucl. Mater. Energy*, 25 (2020), 100842-1-7.

[5] F. Nespoli, K. Tanaka, S. Masuzaki, et al.: A reduced-turbulence regime in the Large Helical Device upon injection of low-Z materials powders, *Nucl. Fusion*, 63:7 (2023), 076001-1-15.

[6] R. Lunsford, S. Masuzaki, F. Nespoli, et al.: Real-time wall conditioning and recycling modification utilizing boron and boron nitride powder injections into the Large Helical Device, *Nucl. Fusion*, 62:8 (2022), 086021-1-14.

[7] M. Shoji, G. Kawamura, et al.: Full-torus impurity transport simulation for optimizing plasma discharge operation using a multi-species impurity powder dropper in the large helical device, *Contrib. Plasma Phys.*, 60 (2020), e201900101-1-7.

[8] Y. Feng, F. Sardei, J. Kisslinger: 3D fluid modelling of the edge plasma by means of a Monte Carlo technique, *J. Nucl. Mater.*, 266-269 (1999), 812-818.

[9] G. Kawamura, Y. Feng, et al.: First EMC3-EIRENE simulations with divertor legs of LHD in realistic device geometry, *Contrib. Plasma Phys.*, 54 (2014), 437-441.

[10] A. Pigarov, R. Smirnov, et al.: Transport of dust particles in tokamak devices, *J. Nucl. Mater.*, 363-365 (2007), 216-221.

[11] R. Smirnov, A. Pigarov, et al.: Modelling of dynamics and transport of carbon dust particles in tokamaks, *Plasma Phys. Control Fusion*, 49:4 (2007), 347-371.

[12] Y. Tanaka, R. Smirnov, A. Pigarov, et al.: Simulation of dynamics of carbon dust particles in the JT-60U tokamak, *J. Nucl. Mater.*, 415 (2011), S1106-S1110.

[13] G. Kawamura, J. Miyazawa, T. Goto, et al.: Application of EMC3-EIRENE to estimation of influence of a liquid metal limiter on an LHD-type fusion plasma, *Plasma Fus. Res.*, 13 (2018), 3403034-1-5.

[14] H. M. Mott-Smith, I. Langmuir: The Theory of Collectors in Gaseous Discharges, *Phys. Rev.*, 28 (1926), 727-763.

[15] A. Pigarov, S. I. Krasheninnikov, et al.: Dust-particle transport in tokamak edge plasmas, *Phys. Plasmas*, 12 (2005), 122508-1-15.

[16] I. Hutchinson: Ion collection by a sphere in a flowing plasma: 3. Floating potential and drag force, *Plasma Phys. Control. Fusion*, 47:1 (2005), 71-87.

[17] I. Hutchinson: Collisionless ion drag force on a spherical grain, *Plasma Phys. Control. Fusion*, 48 (2006), 185-202.

[18] T. Watanabe, Y. Matsumoto, et al.: Magnetic Field Structure and Energetic Particles in the LHD, *Nucl. Fusion*, 46 (2006), 291-305.